nature photonics

Review article

https://doi.org/10.1038/s41566-025-01625-0

MINFLUX achieves molecular resolution with minimal photons

Received: 26 June 2024

Accepted: 14 January 2025

Published online: 6 March 2025

Check for updates

Lukas Scheiderer[1,2,3,5], Zach Marin[1,2,5] & Jonas Ries[1,2,3,4]

Optical super-resolution microscopy is a key technology for structural biology that offers high imaging contrast and live-cell compatibility. Minimal (fluorescence) photon flux microscopy, or MINFLUX, is an emerging super-resolution technique that localizes single fluorophores with high spatiotemporal precision by targeted scanning of a patterned excitation beam featuring a minimum. MINFLUX offers super-resolution imaging with nanometre resolution. When tracking single fluorophores, MINFLUX can achieve nanometre spatial and submillisecond temporal resolution over long tracks, greatly outperforming camera-based techniques. In this Review, we present the basic working principle of MINFLUX and explain how it can reach high photon efficiencies. We then outline the advantages and limitations of MINFLUX, describe recent extensions and variations of MINFLUX and, finally, provide an outlook for future developments.

Continuous advances in electron microscopy over the past century have made it possible to resolve the structures of proteins and their complexes with ångström resolution, even in their native cellular context[1] (Fig. 1a). However, to reach a resolution that is sufficient to identify individual proteins in the electron densities, typically many identical structures need to be averaged. Optical super-resolution microscopy, in comparison, uses fluorescent labels that allow investigation of individual structures without averaging and with high contrast. Unlike electron microscopy, it is applicable to living cells and can directly measure dynamics. In the past two decades, its resolution has been pushed to the molecular scale. Thus, it is becoming an increasingly important complementary technology for structural cell biology[2].

Fluorescence microscopes are among the most important technologies for biology. They use either camera-based detection (widefield microscope) or a scanned laser focus and a point detector in combination with a pinhole for rejecting out-of-focus fluorescence (confocal microscope; Fig. 1b). Their spatial resolution, however, is limited to >200 nm, about half the wavelength λ of the excitation light used and far worse than what is useful for structural biology. The size (standard deviation of the Gaussian approximation, corresponding to the microscope resolution/2.355) of the point spread function (PSF) depends on the numerical aperture (NA) of the objective and is[3]

$$\sigma_{\mathrm{PSF}} = \frac{0.21\lambda}{\mathrm{NA}} \tag{1}$$

Super-resolution microscopy technologies use smart tricks to circumvent this resolution limit for diffraction-unlimited resolution. Stimulated emission depletion (STED) microscopy[4,5] narrows the size of the excitation beam of a confocal microscope by super-positioning of a doughnut-shaped depletion beam that quenches the fluorescence emission outside of the doughnut centre (Fig. 1c). This usually leads to an up to ~10-fold improved spatial resolution, which is determined by the intensity I of the STED laser compared with the saturation intensity I_S, leading to a PSF size of:

$$\sigma_{\mathrm{STED}} = \frac{\sigma_{\mathrm{PSF}}}{\sqrt{1 + I/I_S}}. \tag{2}$$

Single-molecule localization microscopy[6,7] (SMLM) relies on labelling target structures with fluorophores that can be switched between a long-lived dark state and a bright state. On-switching of only a small

[1]Max Perutz Labs, Vienna Biocenter Campus (VBC), Vienna, Austria. [2]University of Vienna, Center for Molecular Biology, Department of Structural and Computational Biology, Vienna, Austria. [3]European Molecular Biology Laboratory, Cell Biology and Biophysics, Heidelberg, Germany. [4]University of Vienna, Faculty of Physics, Vienna, Austria. [5]These authors contributed equally: Lukas Scheiderer, Zach Marin. e-mail: Jonas.ries@univie.ac.at

https://doi.org/10.1038/s41566-025-01625-0

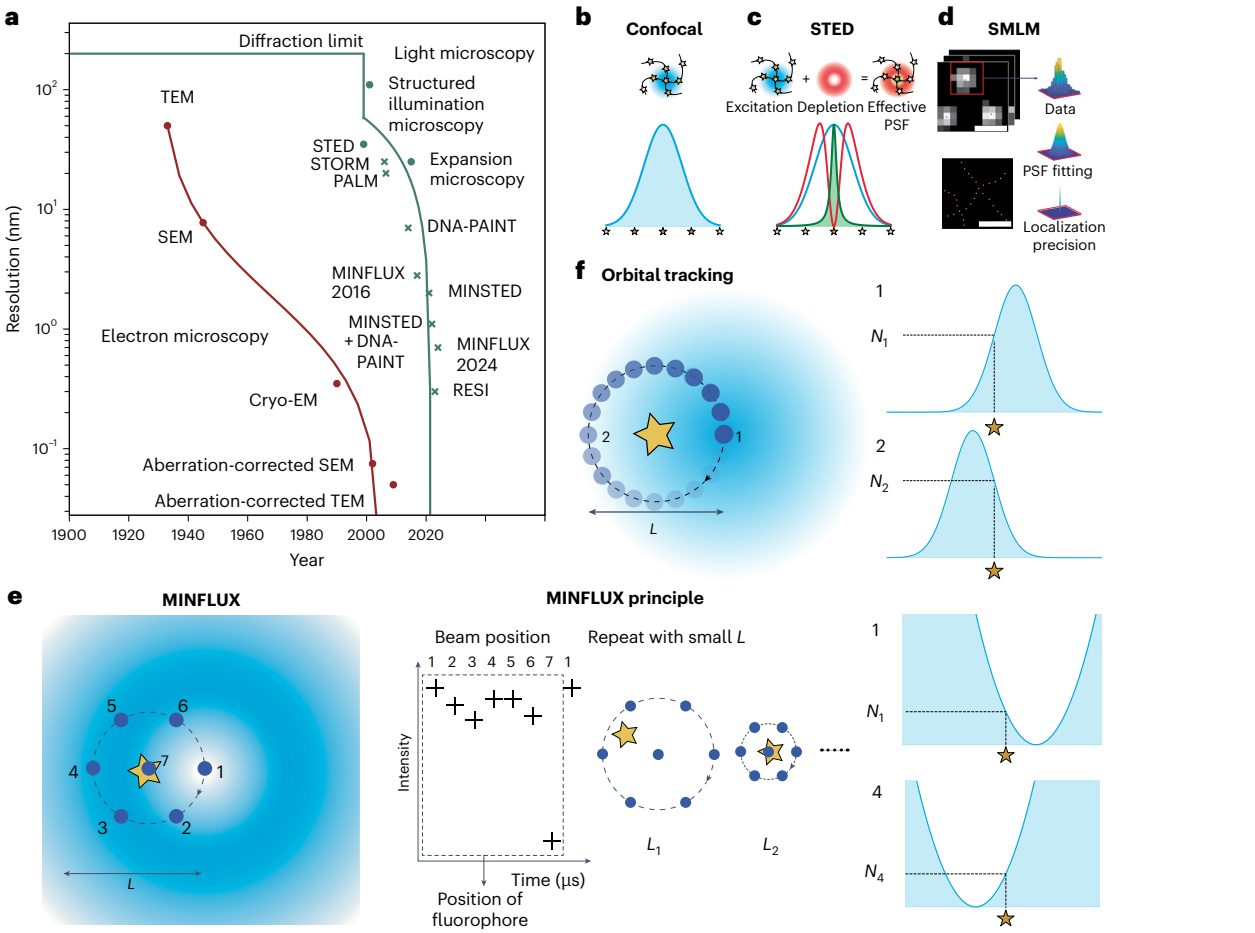

Fig. 1 | Comparison of super-resolution fluorescence microscopy techniques. **a**, Super-resolution fluorescence microscopy has rapidly advanced in the past 20 years[4–7,9,10,12,19,20,34,58–61], approaching the resolution of electron microscopy[62–67] with the advantages of molecular specificity and live-cell compatibility. SMLM methods, including photoactivated localization microscopy (PALM)[6], stochastic optical reconstruction microscopy (STORM)[7,59], DNA-PAINT[9], MINSTED[19] and MINFLUX[12,34], are marked with a cross. SEM, scanning electron microscopy, TEM, transmission electron microscopy. **b**, Confocal microscopy illuminates all fluorophores within the excitation PSF and achieves a resolution of ~200 nm at best. **c**, STED microscopy combines confocal excitation (blue) with a doughnut-shaped depletion beam (red) to quench fluorescence in the periphery, which ensures that only signals from fluorophores at the low-intensity centre (green) are detected, achieving a resolution of ~35 nm. **d**, SMLM uses blinking fluorophores covering the entire field of view, where few fluorophores emit in any single camera frame. Each fluorophore position is determined by fitting to a PSF model. An image with ~5 nm precision is reconstructed from the positions collected across all frames. **e**, MINFLUX uses a doughnut-shaped PSF with a near-zero intensity centre that is sequentially placed at several positions around the fluorophore. From the measured intensities, N_i where i indicates position number, the fluorophore position is estimated. Iterative MINFLUX combines several localization steps with decreasing diameter of the scan path L to achieve single-nanometre localization precisions. A steep PSF gradient combined with low intensities near the doughnut minimum improves the localization precision per photon around fivefold compared with SMLM. **f**, Orbital tracking scans a Gaussian beam circularly around a fluorescent particle with a scan path diameter L to improve particle localization precision by up to ~1.7 times compared with SMLM. The particle position is inferred from measured intensities, which are highly dependent on fluorophore position near the steep portion of the Gaussian PSF. The scan path is continuously re-centred around the fluorophore. Panels **c**–**e** adapted with permission from ref. 2, Annual Reviews.

subset of fluorophores in each of many camera frames leads to sparse images of single fluorophores. Their positions can then be determined with nanometre precision by fitting a model of the PSF to the recorded pixel intensities (Fig. 1d). Because of shot noise, the intensity in each pixel is a random variable from a Poisson distribution, and the localization precision depends strongly on the number of detected fluorescence photons N:

$$\sigma_{SM} = \frac{\sigma_{PSF}}{\sqrt{N}} \quad (3)$$

Under realistic conditions, any fluorescence background degrades σ_{SM}, which can be calculated, for example, as described in Mortensen et al.[8]. The use of fluorophores that emit a large number of photons N leads to a localization precision of a few nanometres[9], and averaging over repeated localizations of the same target protein has pushed the localization precision towards the ångström regime[10]. In contrast to σ_{PSF} and σ_{STED}, which denote the physical size of the PSF, the localization precision σ_{SM} denotes the expectation value of the standard deviation of the fluorophore position.

In SMLM, a super-resolution image is reconstructed by combining millions of fluorophore positions imaged in thousands of camera frames. The principle of precise localization of single emitters with a camera is also key in widefield single-fluorophore tracking techniques[11], which quantify the spatial dynamics of single emitters.

Minimal (fluorescence) photon flux microscopy (MINFLUX)[12], developed in 2017 by the group of Stefan Hell, outperforms the SMLM localization precision limit (equation (3)) by targeted probing of a single fluorophore with a patterned beam that features an intensity minimum (Fig. 1e), reaching unprecedented photon efficiencies.

https://doi.org/10.1038/s41566-025-01625-0

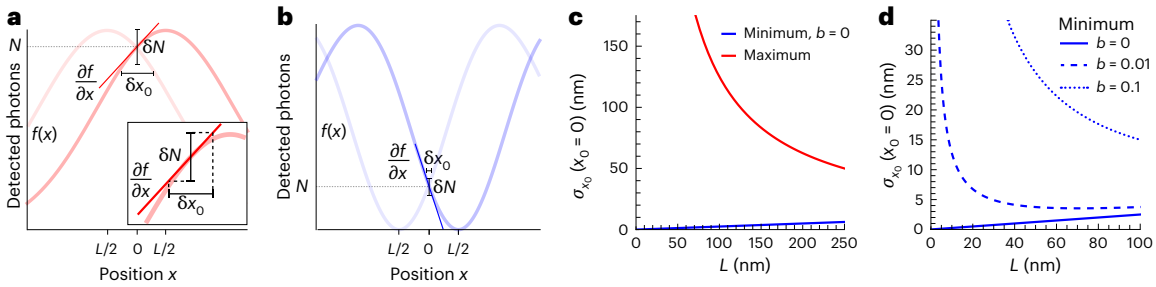

Fig. 2 | Localization with maxima versus minima in one dimension. a, Two maximum PSF measurements at $x_i = \{-L/2, L/2\}$ of an emitter at position $x_0 = 0$. Inset: the position error δx_0 can be calculated from the error δN in measuring the photons N if the gradient of the PSF $\partial f/\partial x$ is known. When the emitter is near the PSF centre, $\delta N = \sqrt{N}$ is large and the gradient is small, resulting in a poor localization precision δx_0. **b**, Two minimum PSF measurements. When the emitter is near the PSF centre, δN is small, and the gradient is large, resulting in a good localization precision δx_0. **c**, Localization precision (Cramér-Rao (lower) bound) for illumination of a fluorophore with two minima versus two maxima. Here, $x_0 = 0$, $b = 0$, $N_{tot} = 100$ photons and $\sigma_{PSF} = 250$ nm. **d**, Even with background, minima outperform maxima PSF measurements. For the minimum case, at $L = 100$, $b = 0.01$ corresponds to a signal-to-background ratio of 3 and $b = 0.1$ corresponds to a signal-to-background ratio of 1.2.

In combination with switchable fluorophores, it allows for SMLM imaging with single-nanometre precision with few photons. For tracking, it can improve the spatial resolution, temporal resolution and track length by around one order of magnitude compared with camera-based techniques.

Principle of MINFLUX

How does MINFLUX achieve a better localization precision than possible with camera-based or confocal detection?

Let us consider a confocal microscope image of a single fluorophore showing the (close-to-Gaussian) PSF of the microscope. PSF fitting of this image would lead to the same localization precision as with a camera (equation (3)). Interestingly, not all pixels in this image carry equal position information: pixels at the flanks of the Gaussian show a strong intensity dependence with small variations of the fluorophore position, whereas pixels at the flat PSF centre carry little position information. If we had prior information on the approximate position of the fluorophore, we could omit the bright, low-information pixels and achieve a similar localization precision with fewer photons from the flanks.

To investigate the precision with which we can determine the position of a fluorophore by targeted probing with focused light, we will consider a simple one-dimensional scheme without background and with a PSF of shape $f(x_0 - x_i)$ positioned at $x_i = 0$. For a fluorophore at position x_0, we detect $N = I_0 f(x_0)$ photons. From such a single measurement, we can retrieve the fluorophore position as $x_0 = f^{-1}(N/I_0)$, provided we know its brightness I_0. In a linear approximation, the error of the position δx is proportional to the error δN in measuring the photons N (Fig. 2a):

$$\delta N = I_0 f'(x_0)\, \delta x_0 \tag{4}$$

Here, $f'(x_0) = \partial f/\partial x|_{x_0}$ is the derivative of f along x, that is, the gradient of the PSF, evaluated at x_0. Because the detection of photons is a Poisson process, $\delta N = \sqrt{N}$. We can substitute $I_0 = N/f(x_0)$ and solve for δx_0:

$$\delta x_0 = \left| \frac{1}{\sqrt{N}} \frac{f(x_0)}{f'(x_0)} \right| \tag{5}$$

where we have taken the absolute value as localization precision is always positive. Thus, in a first approximation, the position error scales inversely with $\sqrt{N}$ and otherwise depends only on the shape of the PSF: both a low-magnitude $f(x)$ and a strong-gradient $f'(x)$ at the emitter position x_0 lead to a good localization precision. For realistic measurements, the fluorophore brightness is typically not known, and we need to perform additional measurements.

The idea of using a strong gradient to localize an emitter is realized in orbital tracking (Fig. 1f), where the steep part of the PSF is scanned in a circular path around an assumed position of a single fluorescent particle (to our knowledge, tracking of targets labelled with single fluorophore molecules has not been demonstrated with this technique)[13–15]. Key for this approach is to iteratively estimate the position of the particle from the intensity variation during the orbital scan and to recentre the midpoint of the circular beam path on the best position estimate. Using a two-dimensional Gaussian approximation of the PSF:

$$I_{max}(\bar{x}_0 - \bar{x}) = I_0 e^{-\frac{(\bar{x}_0 - \bar{x}_i)^2}{2\sigma_{PSF}^2}} \tag{6}$$

with $I_{max}(\bar{x}_0 - \bar{x}_i)$ denoting the intensity measured at position $\bar{x}_i = (x_i, y_i)$, I_0 denoting the amplitude of the excitation beam and $\bar{x}_0$ denoting the position of the emitter, we can calculate the localization precision for a fluorophore that is centred at a circular orbit with a radius $L/2$, in absence of any background fluorescence, as[16]:

$$\sigma_{OT} = \sigma_{SM} \frac{\sqrt{8}\sigma_{PSF}}{L} \tag{7}$$

Thus, we achieve an improvement over diffraction-limited PSF localization if we choose the diameter of the orbit $L > \sqrt{8}\sigma_{PSF}$, which is in agreement with the expected value for orbital radius in the original orbital tracking paper, and the results of probing the fluorophore at the half-maximum of the PSF[13]. In practice, background fluorescence causes a drop in signal-to-background ratio as the Gaussian beam moves away from the fluorophore and a suitable choice is $L \approx 5\sigma_{PSF}$, which results in probing the fluorophore near, but before, where the Gaussian tail flattens[17], leading to an improvement of the localization precision by a factor of $\sigma_{OT} \approx 0.6\sigma_{SM}$.

To improve the localization precision even further, we can generate PSFs with steeper intensity gradients, like the narrow and steep STED PSF. When used for orbital tracking[18], this approach is termed MINSTED[19,20]. An alternative approach is to use a PSF featuring a local intensity minimum with (near-)zero intensity. Here, fluorophores experience a substantial change in excitation intensity with the distance from the minimum, while the intensity at the fluorophore position is still low (Fig. 1e), leading to a high position information per detected photon. This is the principle of MINFLUX.

During a MINFLUX measurement, the minimum of a patterned excitation beam, typically a doughnut beam (not to be confused with

the commonly used doughnut-shaped beam in STED used for depletion instead of excitation) is positioned at different locations around the assumed fluorophore position (Fig. 1e). From the detected number of photons at each location and from the precisely known position of the beam, an improved position estimate can be calculated. In case we have a fluorophore centred in the field of view (FOV), a perfect intensity minimum and no background, the two-dimensional localization precision is[12]

$$\sigma_{\mathrm{MF}} = \frac{L}{\sqrt{8N}} \tag{8}$$

Here, L is the diameter of the scan pattern, which is assumed to be smaller than the size of the PSF, and N is the number of detected photons. Compared with the diffraction-limited localization precision (equation (3)), we gain in two ways: we find an additional factor of $8^{-1/2}$ and the size of the scan pattern L can be chosen much smaller than the PSF size σ_{PSF}.

To intuitively understand why MINFLUX has a high localization precision for a low number of detected photons, let us assume that we already know the position of the fluorophore and can place the dark doughnut centre precisely over it. As the fluorophore does not see any light, we will not detect any photons. But if we move it ever so slightly, it will see some light and emit some photons, and we can easily distinguish no photons from a few photons and from more photons. This is where the high position sensitivity per photon comes from.

So why not simply use an infinitely small L for infinite resolution? The first reason is that in realistic measurements the intensity minimum is not truly zero because of PSF imperfections and fluorescence background. The result is higher shot noise and consequently a worse localization precision, as discussed in detail below. The second reason is that equation (8) is only valid if the fluorophore is close to the centre of the scan pattern, typically within L. But in the beginning of the experiment, only an approximate position of the fluorophore is known and a large L needs to be chosen. This limitation is overcome with iterative MINFLUX[21], which zooms in on the emitter by decreasing L in each iteration while re-centring the scan pattern on the newly estimated position, allowing for a small final L with high localization precision (Fig. 1e). Note that all photons detected during all iterations are part of the total photon budget and should be included in estimations of the photon efficiency.

Let us use the simple one-dimensional localization precision described in equation (equation (5) to examine the difference between measuring a fluorophore position with an intensity maximum (Fig. 2a), as in scanning confocal and orbital tracking, or an intensity minimum (Fig. 2b), as in MINFLUX. For a fixed PSF width determined by the optical system, the maximum shows a larger photon count and therefore a larger uncertainty $\delta N = \sqrt{N}$ than the minimum at the fluorophore position x_0. Furthermore, the gradient of the minimum can be stronger than that of the maximum at this point. We can investigate this analytically by approximating the minimum with a quadratic function

$$I_{\mathrm{min}}(x_0 - x_i) = I_0\left(\frac{(x_0 - x_i)^2}{2\sigma_{\mathrm{q}}^2} + b\right). \tag{9}$$

Here, $I_{\mathrm{min}}(x_0 - x_i)$ denotes the collected intensity, that is, the number of photons, at position x_i, I_0 is a proportionality factor that describes how the brightness of the emitter depends on the illumination laser power, x_0 is the position of the emitter, and σ_{q} parameterizes the steepness of the PSF. b describes a background due to either an imperfect zero of the PSF or autofluorescence of the sample or out-of-focus fluorescence from nearby fluorophores. As all these background contributions scale with the amplitude of the excitation, we multiply b with I_0 in equation (9); thus b itself is independent of the excitation intensity. If we set the background term to zero, we can substitute the one-dimensional case of equations (6) and (9) into equation (5) to see how δx_0 varies as a function of x_0. In this simple scheme

$$\delta x_{0,\mathrm{max}} = \frac{\sigma_{\mathrm{q}}^2}{x_0\sqrt{N}} \text{ and } \delta x_{0,\mathrm{min}} = \frac{x_0}{2\sqrt{N}} \tag{10}$$

For the minimum case, the localization precision $\delta x_{0,\mathrm{min}}$ is improved the closer we measure to the centre of the PSF, whereas $\delta x_{0,\mathrm{max}}$ improves the farther away we measure.

The best achievable localization precision can be calculated as the Cramér-Rao (lower) bound as detailed in Masullo et al.[17]. Here we follow this approach and extract the localization precision σ_{x_0} of the emitter position measurement from the corresponding matrix element. In a realistic experiment, the brightness of the fluorophore and with it the total number of detected photons, $N_{\mathrm{tot}} = \sum N_i$, and the fluorophore position x_0 are unknown. Thus, we need at least two measurements to recover these two unknown parameters. If the background b is not known, we need at least three measurements to determine N_{tot}, x_0 and b (ref. 16). Let us assume that the background is known, and we measure at $x_i = \{-L/2, L/2\}$. Then, we can calculate the localization precision of the minimum case (equation (9)) as[16]

$$\sigma_{\mathrm{min}} = \frac{1}{4L\sqrt{N_{\mathrm{tot}}}} \frac{\left(L^2+4x_0^2+8b\sigma_{\mathrm{q}}^2\right)\sqrt{\left(L^2-4x_0^2\right)^2+16b\sigma_{\mathrm{q}}^2\left(L^2+4x_0^2+4b\sigma_{\mathrm{q}}^2\right)}}{L^2-4x_0^2+8b\sigma_{\mathrm{q}}^2} \tag{11}$$

which reduces to the reported minimum one-dimensional MINFLUX precision[12]

$$\sigma_{\mathrm{MF,1D}} = \sigma_{\mathrm{min}}\left(x_0 = 0, b = 0\right) = \frac{L}{4\sqrt{N_{\mathrm{tot}}}} \tag{12}$$

when $x_0 = 0$ and $b = 0$. Note that this is equivalent to the simple approximation, equation (10), evaluated at $x_0 = L/2$.

We could alternatively localize the same fluorophore with two Gaussian maxima (equation (6)). This results in a precision similar to orbital tracking (equation (7)). We can see (Fig. 2c) that this performs poorly compared with the minimum, as suggested by the simple approximation, even when there is reasonably high background (Fig. 2d).

To summarize, the conceptual requirements for MINFLUX to reach photon-efficient, diffraction-unlimited resolution are:

- Single isolated fluorophores
- A PSF with a near-zero minimum to generate a steep intensity gradient
- Targeted positioning of the PSF in a defined pattern
- Iterative real-time feedback on the position of the scan pattern or sufficiently precise prior information on the fluorophore position

In addition to these fundamental requirements, the success of a MINFLUX experiment depends on several practical requirements and considerations, as follows.

Attaching a fluorophore to the target biomolecule comes with two challenges. First, the labelling process should not influence the function of the protein. Second, the distance of the fluorophore to the target protein should be minimal, otherwise this linkage error will be the main source of the position error rather than the photon limit on localization precision. The common approach of labelling with antibodies can lead to linkage errors of up to 15 nm. Nanobodies, self-labelling enzymes (for example, SNAP-tag or HaloTag), unnatural amino acids or genetic tagging with fluorescent proteins have lower linkage errors and are preferable for MINFLUX[2].

https://doi.org/10.1038/s41566-025-01625-0

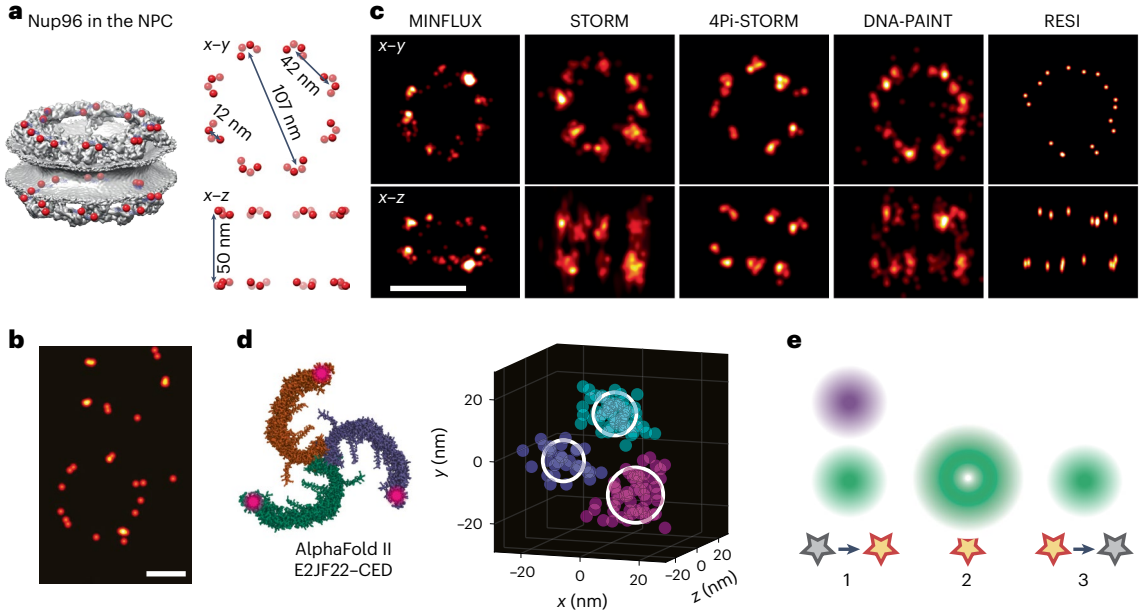

Fig. 3 | MINFLUX imaging achieves molecular resolution. a, Left: electron microscopy density of the nuclear pore complex with C-termini of Nup96 indicated in red. Right: side and top view schematic showing eight-fold symmetry and distances between Nup96 proteins. **b**, Nuclear pore complex imaged in live cells with MINFLUX[21]. **c**, Comparison between different super-resolution techniques imaging Nup96 in nuclear pore complexes in fixed cells: MINFLUX[29], STORM[68], 4Pi-STORM[69], DNA-PAINT and RESI[10]. **d**, Left: structural model of the ion channel PIEZO1. Labels are shown as magenta stars. Right: representative PIEZO1 trimer recorded with 3D MINFLUX. **e**, Proposed targeted activation/deactivation scheme for live-cell imaging. High-intensity ultraviolet activation (purple) is used with the excitation laser (green) until a fluorophore on-switching event is detected, upon which the ultraviolet laser is switched off (1). MINFLUX localization is performed until enough photons are detected (2). High-intensity illumination with the excitation laser quickly switches the fluorophore off (3) and the cycle is repeated. Scale bars, 100 nm. Panels adapted from: **a**, ref. 28, Springer Nature America, Inc; **d**, ref. 38, under a Creative Commons licence CC BY 4.0. Panel **b** reproduced from ref. 21, Springer Nature America, Inc.

Many fluorophores show intensity changes (flickering) on the micro- to millisecond timescale[22,23]. If, for example, the emitter goes to an off-state when the minimum is at a peripheral position, fewer photons will be detected, leading to a wrong position calculation by the MINFLUX estimator[24], which assumes constant intensities. This error can be reduced by averaging over the flickering by using many fast scan cycles for a single localization. Alternatively, one can select more suitable fluorophores for MINFLUX with inherently low flickering and high brightness. Live-cell measurements require live-cell compatible fluorophores and come with the danger that phototoxicity induced by the MINFLUX laser can potentially perturb the process under investigation. In general, the laser intensities in MINFLUX (~10–50 kW cm^{-2}) are comparable to those used in confocal imaging[21] and hence are roughly an order of magnitude higher than that for SMLM[25,26]. But, as the cell is illuminated in only a small region corresponding to the size of the PSF, the average laser intensities a cell sees can be much smaller than in wide-field excitation. In any case, careful controls are necessary to exclude artefacts by photo toxicity in any live-cell fluorescence measurement.

At the nanoscale, the resolution is in many cases limited not only by the number of photons but also by instabilities of the microscope (drift, vibrations), which can easily exceed the nominal localization precision, underscoring the need for extremely precise stabilization of the microscope.

As the signal of the target fluorophore comes from the vicinity of the dark doughnut centre, which is easily outshone by signal generated by perturbing fluorophores illuminated by the bright part of the PSF, the risk of multiple emitters being in their on-state needs to be reduced by activating only a very low fraction of emitters at a time. This is why MINFLUX is implemented with confocal detection, where the pinhole rejects out-of-focus and peripheral fluorescence. For highly dense samples with a substantial (auto-)fluorescent background, MINSTED might be superior to MINFLUX due to its smaller PSF size[27].

MINFLUX imaging

MINFLUX requires low fluorophore densities and low fluorescence background. As such, to use MINFLUX for super-resolution imaging, it needs to be combined with SMLM, that is blinking/photoactivatable fluorophores that are stochastically activated at ultralow densities. The bright fluorophores are sequentially localized by several MINFLUX iterations with successively decreasing L. Because of its higher photon efficiency, MINFLUX can improve the localization precision compared with camera-based SMLM when the resolution is photon limited. This comes at the expense of a much smaller imaged FOV and thus the recording of larger FOVs is slow compared with camera-based techniques. Therefore, precise drift compensation is especially crucial for MINFLUX imaging.

The pioneering work that introduced MINFLUX resolved fluorophore distances of 6 nm on DNA origami, achieving an average localization precision of 1.2 nm with 1,000 photons[12]. In cells, MINFLUX resolved nuclear pore complex test structures[28] with a precision of under 2 nm (refs. 21,29–33), easily showing the 8-fold symmetry of nuclear pore complexes (Fig. 3a). These were the first structures imaged in living cells that provided a clearly superior resolution (Fig. 3b) compared with previous live-cell SMLM[21,28]. On purified proteins, distances in the range of 1–15 nm between up to 4 fluorophores have been measured with ångström precision, demonstrating that MINFLUX can be a powerful alternative to Förster resonance energy transfer (FRET)[34].

As biology is not two-dimensional, the extension of MINFLUX to three dimensions[21,24,29,35,36] was of high importance. In three-dimensional (3D) MINFLUX imaging, a so-called 3D doughnut or bottle beam—effectively a sphere of light with a dark centre—is positioned around the fluorophore in three dimensions to localize it in x, y and z[21,29]. Equally important was the extension of MINFLUX to multiple colours for studying protein interactions and spatial context. Chromatic shifts between

https://doi.org/10.1038/s41566-025-01625-0

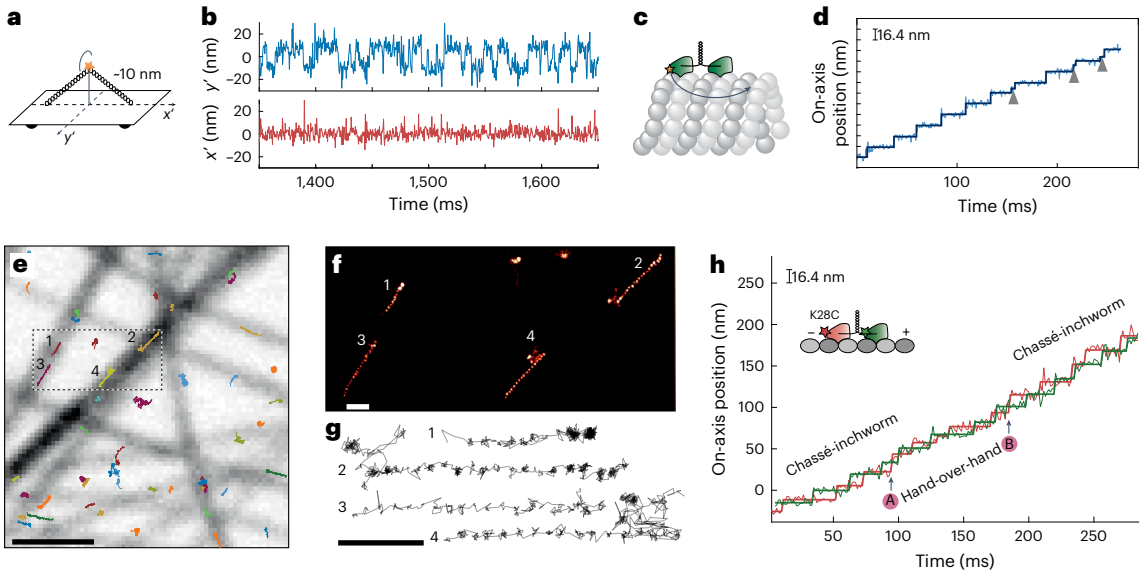

Fig. 4 | MINFLUX tracking follows fast movements. a, Illustration of the DNA origami construct with a single ATTO 647N fluorophore attached at the centre of the bridge (10 nm from the origami base). The emitter can move on a half-circle above the origami and is thus restricted to a projected one-dimensional movement. **b**, MINFLUX traces showing clear oscillation of the fluorophore on the origami along *y*′ and negligible movement along *x*′ with a standard deviation along the principal axis of movement of ~1.7 nm using on average 94 photons detected within 400 µs bins. **c**, Illustration of the molecular motor kinesin-1 with its two heads (green) on a microtubule (grey). **d**, Kinesin-1 trace (1 mM ATP) showing substeps (arrows). The raw data points (faint blue line) are overlaid with a 5 ms moving median filter (bold blue line). **e**, Live-cell tracks of kinesin (HaloTag-K560) show 16 nm steps. Coloured tracks are overlaid with confocal images of the microtubules. Scale bar, 1 µm. **f**,**g**, The tracks indicated in **e** rendered as a super-resolution image (**f**) and line plots connecting localizations (**g**), showing clear walking steps (localization precision, 2 nm; temporal resolution, 1 ms). Scale bars, 100 nm. **h**, One-dimensional dual-colour trace of kinesin, walking in an in vitro microtubule assay. The heads are labelled with different dyes and tracked simultaneously. Between A and B, kinesin walks in a hand-over-hand mode with the rear always overtaking the leading head. The other parts of the trace are best explained by a chassé-inchworm mechanism, where the rear lags the leading head. Panels adapted with permission from: **a**,**b**, ref. 39, PNAS; **d**, ref. 44, AAAS; **e**–**g**, ref. 45, AAAS; **h**, ref. 47, under a Creative Commons licence CC BY 4.0.

the colour channels can be minimized by using spectrally close fluorophores that are excited with the same wavelength, and emission events are assigned to the respective fluorophore depending on the ratio obtained from spectral splitting with a dichroic mirror. Using this approach, Pape et al. investigated the proximity of different mitochondrial subcomplexes[35].

Combined with DNA point accumulation in nanoscale topography (DNA-PAINT)[9], where fluorophores transiently attach to the target via DNA strands, MINFLUX can record multicolour images of fixed cells by sequentially using different DNA strands for different targets. However, for such bright labels, the advantage of MINFLUX compared with camera-based approaches diminishes. For example, the camera-based DNA-PAINT approach resolution enhancement by sequential imaging (RESI)[10], which sequentially images sparse target subsets at moderate spatial resolution and then averages localizations in close proximity in each of these subsets, achieved ångström resolution on large FOVs (Fig. 3c).

Commercialization of MINFLUX boosted the accessibility of the technology[29] and allowed its application to numerous biological systems including the photoreceptor active zone[36] and the injectiosome, a bacterial molecular machine[37]. Furthermore, statistical analysis of MINFLUX images of the PIEZO1 ion channel resolved few-nanometre conformational shifts caused by chemical and mechanical modulators, giving better insight into the activation of the mechanosensitive channel[38] (Fig. 3d).

MINFLUX imaging shows its full potential when fluorophores of low brightness need to be used[21], when small FOVs are sufficient and when labelling schemes with minimal linkage error can be employed. Although it has provided nice results on fixed samples, MINFLUX is hard to use for dynamic imaging in live cells because of its slow speed. Any motion of the target structure of more than the localization precision within the measurement time will lead to motion blur. However, as the measurement time scales with the FOV, tiny regions of interest, for example, a single nuclear pore complex, can be imaged relatively quickly (Fig. 3b). In the future, MINFLUX has the potential to outperform SMLM for dynamic live-cell imaging with a targeted activation/deactivation approach (Fig. 3e): here, photoswitchable fluorophores are illuminated with a high intensity of the ultraviolet and imaging laser. After the on-switching of a fluorophore, the ultraviolet laser is stopped to avoid activation of a second fluorophore. After its localization and off-switching/bleaching with the imaging laser, the next emitter can be activated and localized in rapid succession. Such an approach necessitates new and faster microscopes, but most importantly live-cell compatible fluorophores that perform well for MINFLUX and that can be switched on rapidly by light. However, for imaging of protein assemblies in fixed cells, there might be only a few applications where MINFLUX will outperform state-of-the art SMLM (Fig. 3c), for example, when imaging photoactivatable fluorescent proteins or when high 3D resolution is required.

MINFLUX tracking

An application where MINFLUX already clearly outperforms camera-based localization is single-fluorophore tracking. During MINFLUX tracking, the position of the scan pattern is recentred to the estimated fluorophore position after each iteration and thus the MINFLUX pattern effectively follows the fluorophore. Compared with camera-based tracking, the high photon efficiency leads to three advantages: a high spatial precision with few detected photons, high temporal resolution because detection of fewer photons is faster and long tracks because the fluorophore close to the dark doughnut centre is not bleached quickly. The drawback is that ultralow fluorophore concentrations are required.

https://doi.org/10.1038/s41566-025-01625-0

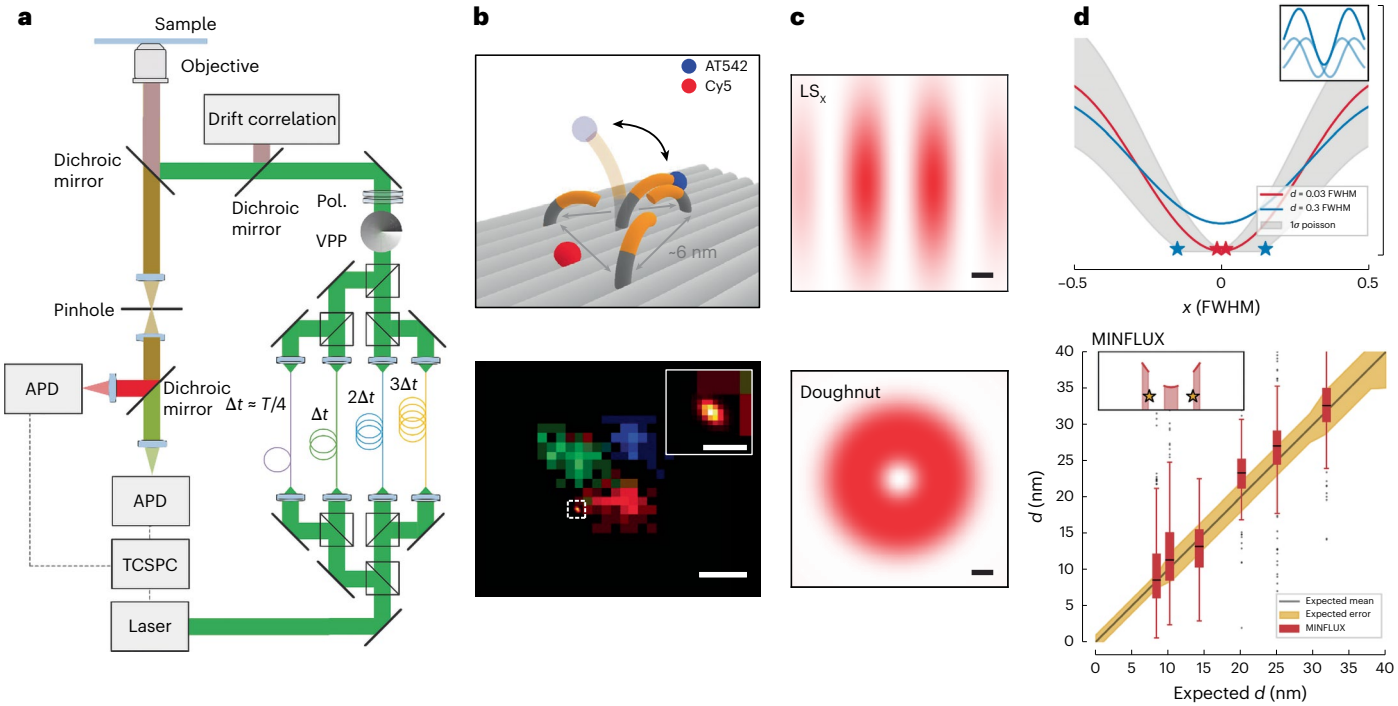

Fig. 5 | New approaches to MINFLUX with simplified set-ups, alternative PSF shapes and multi-emitter separation. a, Illustration of the pMINFLUX set-up. A pulsed laser is split into four beams and coupled into optical fibres, which delay the laser pulses. The beams are recombined, and doughnut-shaped beams are created with a vortex phase plate (VPP). The beams are focused onto the sample in a triangular pattern with one beam in the centre of the triangle. APD, avalanche photodiode; Pol., polarization optics; TCSPC, time-correlated single photon counting unit; Δ*t*, time delay; *T*, period of original pulse train. **b**, Super-resolved FRET in pMINFLUX. Top: illustration of the dynamic DNA origami with three protruding strands spaced ~6 nm apart, to which an ATTO 542 (AT542)-labelled DNA pointer transiently hybridizes. Bottom: MINFLUX localizations of the DNA pointer (blue, green, red). Scale bar, 5 nm. Inset: the position of Cy5 was deduced from the calculated FRET distances. Scale bar, 1 nm. **c**, Comparison of the line-shaped minimum LS_x and doughnut excitation intensity distribution in the focal plane. Scale bars, 100 nm. **d**, Multi-emitter MINFLUX. Top: two non-blinking emitters/scatterers (shown as stars) of the same colour can be localized simultaneously below the diffraction limit as one of them can be 'turned off' by the excitation minimum. Inset: the profile of the average intensity profiles of each point scatterer and their joint signal. Bottom: boxplot of the measured over the expected distances *d* between fluorophores on nanorulers of different lengths. Recording the photons originating near the illumination minimum (see inset) suffices to separate simultaneously emitting fluorophores down to 8 nm. The boxes extend from the lower to upper quartile values of the data. Error bars mark the interval from the median (black line within box) to the last point within a 1.5 interquartile range (IQR). Outliers are shown as black dots. FWHM, full-width at half-maximum. Panels adapted with permission from: **a**,**b**, ref. 49, Springer Nature, Ltd.; **c**, ref. 44, AAAS; **d**, ref. 56, under a Creative Commons licence CC BY 4.0.

The first MINFLUX study demonstrated tracking of single 30S ribosomal subunits labelled with a fluorescent protein in living bacteria[12]. On DNA origami test structures (Fig. 4a), MINFLUX tracking achieved a localization precision of ~2 nm with a 400 µs time resolution using <100 fluorescent photons per localization[39] (Fig. 4b).

Because single-colour tracking cannot easily distinguish conformational changes of proteins from overall motion, it is especially useful to study either diffusion[12,29] or conformational changes when the overall motion is well defined, as for motor proteins such as kinesin (Fig. 4c). Its stepping motion has been studied extensively in vitro on purified proteins[40–43], but many details are still debated, for example, due to the large (bead) label size or low temporal resolution of the established techniques. Some of these controversies have been resolved by MINFLUX's high spatio-temporal resolution combined with a small fluorophore label. For example, kinesin substeps lasting only a few milliseconds were observed via MINFLUX tracking (Fig. 4d) and it was concluded that this motor protein binds its fuel, ATP, during this state[44]. Furthermore, a concurrent rightwards rotation of the so-called heads and a rotation of the stalk were identified by observing fast movements on the scale of only a few nanometres. A switching of protofilament lanes was observed on purified proteins[27] and in fixed cells[45].

Because of insufficient spatial and temporal resolution of live-cell compatible tracking techniques, kinesin stepping had not been previously observed directly in cells. Live-cell MINFLUX tracking (Fig. 4e–g) overcame this limitation and resolved the 16 nm steps in 2 dimensions and in 3 dimensions[45] and allowed characterizing step size and dwell time distributions. In addition, motors were tracked in motorPAINT[46], where labelled motors walk on microtubules of fixed and permeabilized cells, and were used to map out cellular microtubules with down to protofilament resolution.

Dual-colour MINFLUX co-tracking[47,48] will be the next transformative development of MINFLUX, as it allows studying conformational changes of proteins during their action, ultimately in living cells. Labelling of two parts of a protein or protein complex with two different dyes and tracking them simultaneously allows for determining of their relative positions with nanometre spatial and (sub-)millisecond temporal resolution. A first implementation of MINFLUX co-tracking[47] using an in vitro assay observed conformational changes that suggest a novel walking mode of kinesin-1 (Fig. 4h), highlighting the potential of MINFLUX to enable biological insights.

New approaches to MINFLUX

MINFLUX is a new technology, and the development of improved concepts, implementations and analysis approaches is already an active field of research. In the following, we discuss new technical implementations that will improve the performance and accessibility of MINFLUX and enable novel applications.

With a spatial resolution in the single-nanometre range, MINFLUX rivals FRET in studying small distances between fluorophores, with the added advantage that the MINFLUX distance measurement is absolute and not limited in scale[34]. Pulsed interleaved MINFLUX (p-MINFLUX) allows for simultaneous MINFLUX and FRET tracking[49] (Fig. 5a,b). The microscope was implemented by modifying the excitation path of a time-correlated single-photon counting confocal microscope[50] and performing fast scanning by using four beam paths of different lengths, so that the laser pulses arrive at the four scanning positions at different times. The advantage is a simple set-up, but this comes at the expense of flexibility, as the scan size L cannot be changed during the experiment—hence, zooming-in on the fluorophore to increase photon efficiency is not possible.

Simplifying MINFLUX microscopes will be key to enable more groups to endeavour in technical developments and to give access to the many potential biological users. An important step in this direction was the simple extension of standard confocal microscopes with minor modifications to enable MINFLUX-like measurements in a technique called single-molecule localization by RASTer scanning a MINimum of light (RASTMIN)[51], although it remains to be seen whether such an implementation has sufficient flexibility to unlock the full potential of MINFLUX. The development of a fast variable phase plate has the potential to enable multi-colour 3D MINFLUX with a stable and simple set-up[24].

Although MINFLUX is often associated with a doughnut-shaped PSF, it is by no means necessary and alternative PSFs featuring a local minimum might even outperform doughnut-based MINFLUX[24,44] (Fig. 5c). Using destructive interference of two laser beams in the focus creates a line of minimum intensity that can be quickly scanned by changing the phase of one of the beams[44]. In a similar way, a bi-lobed PSF can be generated and scanned rapidly by a variable phase plate[24]. This allows for a one-dimensional MINFLUX localization. To enable two-dimensional and 3D MINFLUX, separate patterns for each dimension are used sequentially. 4Pi-MINFLUX[52] creates striped PSFs along 3 directions and comes with the advantage of doubling the detection efficiency by using 2 opposing objectives and hence achieving the highest 3D precision per detected photon so far (0.5 nm, 0.5 nm and 0.3 nm in the x, y and z directions, respectively, for ~400 photons per dimension).

Because only a single beam is used, the strongest limitations on MINFLUX are low throughput and long measuring times. Acquisitions could be markedly sped up by parallelization, that is, simultaneous imaging with multiple beams. This is challenging, as the scan path of each beam would need to be updated in real time and centred at the corresponding fluorophore. Modulation-enhanced SMLM methods[53–55] can be thought of as a combination of structured illumination microscopy with SMLM. However, as they lack fluorophore-specific feedback, they achieve, on average, only twofold improvements in resolution over SMLM and thus cannot be considered parallelized versions of MINFLUX.

MINFLUX needs ultralow concentrations of fluorophores because background fluorophores in the periphery of the doughnut can easily be much brighter than the fluorophore of interest at the intensity minimum. Interestingly, it has been demonstrated that multiple fluorophores of the same colour can be resolved with multi-emitter MINFLUX, provided that they are in close vicinity[56]. For multi-emitter fitting in SMLM, the added shot noise of both fluorophores quickly degrades the precision[57]. In contrast, keeping the fluorophores close to the minimum in MINFLUX, where one of the fluorophores can effectively be 'turned off' when centred at the minimum, allows for a far better separation than in multi-emitter SMLM (Fig. 5d). This approach could become a useful alternative to multi-colour co-tracking, as it allows tracking distances among several positions on a single protein labelled with the same colour. It needs to be seen how this approach performs under the high background conditions found in living cells and how it scales with the number of emitters.

Conclusion

Because of its photon efficiency in localizing single fluorophores, MINFLUX has a high potential to become a key technology for structural biology, ideally complementing electron microscopy and other super-resolution techniques. In fixed cells, it reveals precise arrangements of proteins, but optimized SMLM techniques with bright labels currently achieve a similar, if not better, resolution[10] combined with a much larger FOV. The standout feature of MINFLUX imaging might become fast live-cell imaging of cellular structures in a small FOV. Currently, the most transformative impact of MINFLUX is in single-fluorophore tracking, with the development of multi-colour co-tracking opening the possibility to directly watch conformational changes of proteins performing their functions in living cells.

As a young technology, MINFLUX is continuously evolving. To become a standard technique with high impact in structural biology, several challenges still need to be overcome. Live-cell MINFLUX would greatly profit from improved fluorophores for dynamic live-cell imaging and higher robustness against autofluorescent background and higher labelling densities. Multi-fluorophore tracking, using either separate colours or multi-emitter MINFLUX, is limited by the need for very high labelling efficiencies (so that a sufficiently high fraction of targets is labelled in all colours) in combination with ultralow densities, which is difficult to control in living cells. Throughput is still much lower compared with camera-based techniques and new parallelization approaches, especially for imaging of larger structures, will be crucial to reduce measurement times to acceptable levels. Often, the accuracy in MINFLUX experiments is not limited by the detected photons, but by instabilities of the set-up. Thus, ultrastable microscopes will be key to reach the full potential of MINFLUX. In-depth theoretical analysis of the MINFLUX principle in combination with simulations might yield a way to improve accuracy, robustness and throughput of the technique.

Commercialization of MINFLUX has improved accessibility and ease of use. Further reducing the complexity and difficulty of MINFLUX experiments will help to enable non-expert users to obtain data of the highest quality. The development of a robust, affordable and easy-to-build open-source MINFLUX system would further spread the use of this technology to researchers for which a commercial system is out of reach.

With these developments, the future of MINFLUX looks bright as a standard technique for structural biology that can bring molecular resolution to the living cell.

References

1. Saibil, H. R. Cryo-EM in molecular and cellular biology. *Mol. Cell* **82**, 274–284 (2022).
2. Liu, S., Hoess, P. & Ries, J. Super-resolution microscopy for structural cell biology. *Annu. Rev. Biophys.* **51**, 301–326 (2022).
3. Zhang, B., Zerubia, J. & Olivo-Marin, J.-C. Gaussian approximations of fluorescence microscope point-spread function models. *Appl. Opt.* **46**, 1819–1829 (2007).
4. Hell, S. W. & Wichmann, J. Breaking the diffraction resolution limit by stimulated emission: stimulated-emission-depletion fluorescence microscopy. *Opt. Lett.* **19**, 780–782 (1994).
5. Klar, T. A., Jakobs, S., Dyba, M., Egner, A. & Hell, S. W. Fluorescence microscopy with diffraction resolution barrier broken by stimulated emission. *Proc. Natl Acad. Sci. USA* **97**, 8206–8210 (2000).
6. Betzig, E. et al. Imaging intracellular fluorescent proteins at nanometer resolution. *Science* **313**, 1642–1645 (2006).
7. Rust, M. J., Bates, M. & Zhuang, X. Sub-diffraction-limit imaging by stochastic optical reconstruction microscopy (STORM). *Nat. Methods* **3**, 793–796 (2006).
8. Mortensen, K. I., Churchman, L. S., Spudich, J. A. & Flyvbjerg, H. Optimized localization analysis for single-molecule tracking and super-resolution microscopy. *Nat. Methods* **7**, 377–381 (2010).

9. Jungmann, R. et al. Multiplexed 3D cellular super-resolution imaging with DNA-PAINT and Exchange-PAINT. *Nat. Methods* **11**, 313–318 (2014).
10. Reinhardt, S. C. M. et al. Ångström-resolution fluorescence microscopy. *Nature* **617**, 711–716 (2023).
11. Yildiz, A. & Selvin, P. R. Fluorescence imaging with one nanometer accuracy: application to molecular motors. *Acc. Chem. Res.* **38**, 574–582 (2005).
12. Balzarotti, F. et al. Nanometer resolution imaging and tracking of fluorescent molecules with minimal photon fluxes. *Science* **355**, 606–612 (2017).
13. Enderlein, J. Tracking of fluorescent molecules diffusing within membranes. *Appl. Phys. B* **71**, 773–777 (2000).
14. Levi, V., Ruan, Q., Kis-Petikova, K. & Gratton, E. Scanning FCS, a novel method for three-dimensional particle tracking. *Biochem. Soc. Trans.* **31**, 997–1000 (2003).
15. Levi, V., Ruan, Q. & Gratton, E. 3-D particle tracking in a two-photon microscope: application to the study of molecular dynamics in cells. *Biophys. J.* **88**, 2919–2928 (2005).
16. Marin, Z. & Ries, J. Approximations of MINFLUX localization precision with background. Preprint at http://arxiv.org/abs/2410.12427 (2024).
17. Masullo, L. A., Lopez, L. F. & Stefani, F. D. A common framework for single-molecule localization using sequential structured illumination. *Biophys. Rep.* **2**, 100036 (2022).
18. Vallmitjana Lees, A. & Gratton, E. 3D orbital tracking under STED microscopy. *Biophys. J.* **116**, 440a (2019).
19. Weber, M. et al. MINSTED fluorescence localization and nanoscopy. *Nat. Photon.* **15**, 361–366 (2021).
20. Weber, M. et al. MINSTED nanoscopy enters the ångström localization range. *Nat. Biotechnol.* **41**, 569–576 (2023).
21. Gwosch, K. C. et al. MINFLUX nanoscopy delivers 3D multicolor nanometer resolution in cells. *Nat. Methods* **17**, 217–224 (2020).
22. Huang, Z. et al. Spectral identification of specific photophysics of Cy5 by means of ensemble and single molecule measurements. *J. Phys. Chem. A* **110**, 45–50 (2006).
23. Haupts, U., Maiti, S., Schwille, P. & Webb, W. W. Dynamics of fluorescence fluctuations in green fluorescent protein observed by fluorescence correlation spectroscopy. *Proc. Natl Acad. Sci. USA* **95**, 13573–13578 (1998).
24. Deguchi, T. & Ries, J. Simple and robust 3D MINFLUX excitation with a variable phase plate. *Light Sci. Appl.* **13**, 134 (2024).
25. Jones, S. A., Shim, S.-H., He, J. & Zhuang, X. Fast, three-dimensional super-resolution imaging of live cells. *Nat. Methods* **8**, 499–508 (2011).
26. Shroff, H., Galbraith, C. G., Galbraith, J. A. & Betzig, E. Live-cell photoactivated localization microscopy of nanoscale adhesion dynamics. *Nat. Methods* **5**, 417–423 (2008).
27. Scheiderer, L., Von Der Emde, H., Hesselink, M., Weber, M. & Hell, S. W. MINSTED tracking of single biomolecules. *Nat. Methods* **21**, 569–573 (2024).
28. Thevathasan, J. V. et al. Nuclear pores as versatile reference standards for quantitative superresolution microscopy. *Nat. Methods* **16**, 1045–1053 (2019).
29. Schmidt, R. et al. MINFLUX nanometer-scale 3D imaging and microsecond-range tracking on a common fluorescence microscope. *Nat. Commun.* **12**, 1478 (2021).
30. Ostersehlt, L. M. et al. DNA-PAINT MINFLUX nanoscopy. *Nat. Methods* **19**, 1072–1075 (2022).
31. Remmel, M., Scheiderer, L., Butkevich, A. N., Bossi, M. L. & Hell, S. W. Accelerated MINFLUX Nanoscopy, through spontaneously fast-blinking fluorophores. *Small* **19**, 2206026 (2023).
32. Lincoln, R. et al. A general design of caging-group-free photoactivatable fluorophores for live-cell nanoscopy. *Nat. Chem.* **14**, 1013–1020 (2022).
33. Remmel, M. et al. Photoactivatable xanthone (PaX) dyes enable quantitative, dual color, and live-cell MINFLUX nanoscopy. *Small Methods* https://doi.org/10.1002/smtd.202301497 (2024).
34. Sahl, S. J. et al. Direct optical measurement of intramolecular distances with angstrom precision. *Science* **386**, 180–187 (2024).
35. Pape, J. K. et al. Multicolor 3D MINFLUX nanoscopy of mitochondrial MICOS proteins. *Proc. Natl Acad. Sci. USA* **117**, 20607–20614 (2020).
36. Grabner, C. P. et al. Resolving the molecular architecture of the photoreceptor active zone with 3D-MINFLUX. *Sci. Adv.* **8**, eabl7560 (2022).
37. Carsten, A. et al. MINFLUX imaging of a bacterial molecular machine at nanometer resolution. *Methods. Appl. Fluoresc.* **11**, 015004 (2023).
38. Mulhall, E. M. et al. Direct observation of the conformational states of PIEZO1. *Nature* **620**, 1117–1125 (2023).
39. Eilers, Y., Ta, H., Gwosch, K. C., Balzarotti, F. & Hell, S. W. MINFLUX monitors rapid molecular jumps with superior spatiotemporal resolution. *Proc. Natl Acad. Sci. USA* **115**, 6117–6122 (2018).
40. Schnitzer, M. J. & Block, S. M. Kinesin hydrolyses one ATP per 8-nm step. *Nature* **388**, 386–390 (1997).
41. Yildiz, A., Tomishige, M., Vale, R. D. & Selvin, P. R. Kinesin walks hand-over-hand. *Science* **303**, 676–678 (2004).
42. Mickolajczyk, K. J. et al. Kinetics of nucleotide-dependent structural transitions in the kinesin-1 hydrolysis cycle. *Proc. Natl Acad. Sci. USA* **112**, E7186–E7193 (2015).
43. Isojima, H., Iino, R., Niitani, Y., Noji, H. & Tomishige, M. Direct observation of intermediate states during the stepping motion of kinesin-1. *Nat. Chem. Biol.* **12**, 290–297 (2016).
44. Wirth, J. O. et al. MINFLUX dissects the unimpeded walking of kinesin-1. *Science* **379**, 1004–1010 (2023).
45. Deguchi, T. et al. Direct observation of motor protein stepping in living cells using MINFLUX. *Science* **379**, 1010–1015 (2023).
46. Tas, R. P. et al. Differentiation between oppositely oriented microtubules controls polarized neuronal transport. *Neuron* **96**, 1264–1271.e5 (2017).
47. Scheiderer, L., Wirth, J. O., Tarnawski, M. & Hell, S. W. Dual-color MINFLUX: kinesin-1 takes Chassé-inchworm steps. Preprint at *bioRxiv* https://doi.org/10.1101/2024.03.05.583551 (2024).
48. Geismann, M. K., Gomez-Segalas, A., Passera, A., Shirzadian, M. & Balzarotti, F. A fast interferometric beam shaper for multi-emitter 3D MINFLUX. Preprint at *bioRxiv* https://doi.org/10.1101/2023.12.09.570565 (2024).
49. Cole, F. et al. Super-resolved FRET and co-tracking in pMINFLUX. *Nat. Photon.* https://doi.org/10.1038/s41566-024-01384-4 (2024).
50. Masullo, L. A. et al. Pulsed interleaved MINFLUX. *Nano Lett.* **21**, 840–846 (2021).
51. Masullo, L. A. et al. An alternative to MINFLUX that enables nanometer resolution in a confocal microscope. *Light Sci. Appl.* **11**, 199 (2022).
52. Rickert, J. D., Held, M. O., Engelhardt, J. & Hell, S. W. 4Pi MINFLUX arrangement maximizes spatio-temporal localization precision of fluorescence emitter. *Proc. Natl Acad. Sci. USA* **121**, e2318870121 (2024).
53. Cnossen, J. et al. Localization microscopy at doubled precision with patterned illumination. *Nat. Methods* **17**, 59–63 (2020).
54. Gu, L. et al. Molecular resolution imaging by repetitive optical selective exposure. *Nat. Methods* **16**, 1114–1118 (2019).
55. Jouchet, P. et al. Nanometric axial localization of single fluorescent molecules with modulated excitation. *Nat. Photon.* **15**, 297–304 (2021).
56. Hensel, T. A., Wirth, J. O., Schwarz, O. L. & Hell, S. W. Diffraction minima resolve point scatterers at few hundredths of the wavelength. *Nat. Phys.* https://doi.org/10.1038/s41567-024-02760-1 (2025).

57. Schoen, I. Localization precision in stepwise photobleaching experiments. *Biophys. J.* **107**, 2122–2129 (2014).
58. Gustafsson, M. G. L. Surpassing the lateral resolution limit by a factor of two using structured illumination microscopy. *J. Microsc.* **198**, 82–87 (2000).
59. Diekmann, R. et al. Optimizing imaging speed and excitation intensity for single-molecule localization microscopy. *Nat. Methods* **17**, 909–912 (2020).
60. Chen, F., Tillberg, P. W. & Boyden, E. S. Expansion microscopy. *Science* **347**, 543–548 (2015).
61. Hümpfer, N., Thielhorn, R. & Ewers, H. Expanding boundaries—a cell biologist's guide to expansion microscopy. *J. Cell Sci.* **137**, jcs260765 (2024).
62. Ruska, E. The development of the electron microscope and of electron microscopy. *Biosci. Rep.* **7**, 607–629 (1987).
63. Muller, D. A. Structure and bonding at the atomic scale by scanning transmission electron microscopy. *Nat. Mater.* **8**, 263–270 (2009).
64. Taylor, K. A. & Glaeser, R. M. Electron microscopy of frozen hydrated biological specimens. *J. Ultrastruct. Res.* **55**, 448–456 (1976).
65. Henderson, R. et al. Model for the structure of bacteriorhodopsin based on high-resolution electron cryo-microscopy. *J. Mol. Biol.* **213**, 899–929 (1990).
66. Batson, P. E., Dellby, N. & Krivanek, O. L. Sub-ångström resolution using aberration corrected electron optics. *Nature* **418**, 617–620 (2002).
67. Kisielowski, C. et al. Detection of single atoms and buried defects in three dimensions by aberration-corrected electron microscope with 0.5-Å information limit. *Microsc. Microanal.* **14**, 469–477 (2008).
68. Wu, Y.-L. et al. Maximum-likelihood model fitting for quantitative analysis of SMLM data. *Nat. Methods* **20**, 139–148 (2023).
69. Li, Y. et al. Global fitting for high-accuracy multi-channel single-molecule localization. *Nat. Commun.* **13**, 3133 (2022).

Acknowledgements

We thank S. Liu, N. Sergeev, T. Deguchi and F. Reina for helpful discussions. This work was supported by the European Research Council (grant number ERC CoG-724489 to J.R.).

Author contributions

All authors contributed to literature research, discussion, writing and editing of the paper.

Competing interests

The authors declare no competing interests.

Additional information

Correspondence and requests for materials should be addressed to Jonas Ries.

Peer review information *Nature Photonics* thanks the anonymous reviewers for their contribution to the peer review of this work.

Reprints and permissions information is available at www.nature.com/reprints.

Publisher's note Springer Nature remains neutral with regard to jurisdictional claims in published maps and institutional affiliations.